Journal of Materials Chemistry A

RSC Publishing

PAPER

View Article Online
View Journal | View Issue

Cite this: J. Mater. Chem. A, 2013, 1, 11880

Pt–CuS heterodimers by sulfidation of CuPt alloy nanoparticles and their selective catalytic activity toward methanol oxidation†

Xianguang Ding,[abc] Yu Zou,[a] Feng Ye,[d] Jun Yang*[d] and Jiang Jiang*[a]

Received 25th May 2013
Accepted 5th August 2013

DOI: 10.1039/c3ta12049j

www.rsc.org/MaterialsA

Hybrid nanostructures can combine two or more functionalities in one unit and oftentimes exhibit synergistically enhanced properties compared to the simple sum of the constituents. Herein, we demonstrate the facile synthesis of Pt–CuS heterogeneous nanoparticle dimers based on the sulfidation of the corresponding bimetallic alloy templates. It begins with the preparation of CuPt alloy nanoparticles in an organic solvent, which are then converted into Pt–CuS heterodimers by reacting with elemental sulfur in octadecene at elevated temperatures. The Pt–CuS heterodimers display highly selective activity for catalyzing the methanol oxidation reaction at room temperature due to the strong electronic coupling effect between the different domains in the heterodimers. The structural transformation from alloy to heterogeneous nanomaterials may provide new opportunities to design and fabricate hybrid nanostructures with interesting physicochemical properties.

Introduction

Metal–semiconductor hybrid nanoparticles with core–shell or heterostructure geometry have become one of the key research focuses of nanotechnology due to their unique properties. As hybrid structures can combine two or more functionalities in one unit and oftentimes exhibit synergistically enhanced properties compared to the simple sum of the constituents,[1–4] they have become excellent candidates for a wide range of applications especially in catalysis[5–7] and as building blocks in electronic devices.[8] For example, in core–shell CdSe@Pt nanohybrids obtained by reducing platinum precursors with sodium citrate in the presence of preformed CdSe nanocrystals, the compressive strain effect of the CdSe core on the deposited Pt shell resulted in an appropriate downshift of the d-band center of Pt catalysts, which is favourable for catalyzing the oxygen reduction and methanol oxidation in direct methanol fuel cells.[9]

Seeded growth is the most developed method in creating hybrid nanoparticles,[10–18] where the formation and geometry of the hybrid structure largely depend on the lattice constants of constituent materials and their interfacial energy.[19,20] Moreover, the size of the seeds,[21–23] concentration and ratio of precursors of second materials to the seed nanoparticles, the surface chemistry of seeds,[10,11] and the reaction temperature[16,24] can also affect the hybrid structure formation, and these factors complicate the hybrid nanostructure synthesis. The Banin group and the Alivisatos group conducted pioneering work on growing noble metal tips on cadmium chalcogenide nanocrystals using a solution phase method, in which case light also played a critical role.[13,25,26]

With less reaction variables to tune compared to the seeded growth method, nanoparticle templated conversion has become an emerging technique in fabricating compositional and morphological controlled nanocrystals.[27] Yin *et al.* first synthesized Pt@CoO yolk–shell nanoparticles utilizing the Kirkendall effect at the nanoscale.[28] The Schaak group[29] and our group[30] observed the formation of Au–Cu_2S heteromers by treating AuCu alloy nanoparticles with sulfur and dodecanethiol, respectively. Recently, Wang *et al.* synthesized several noble metal–semiconductor hybrids with different geometries by reacting metal core–shell or metal alloy nanoparticles with sulfur.[31] These studies demonstrated the simplicity and versatility of the nanoparticle template based chemical conversion method in synthesizing metal–metal oxide (sulfide) hybrid nanostructures.

Cu_2S and its nonstoichiometry copper-deficient form $Cu_{2-x}S$, due to a suitable bulk band gap of 1.21 eV and strong plasmonic absorption in the near-infrared (NIR) region,[32] have been investigated as promising photovoltaic materials,[33,34] photocatalysts,[35] for gas sensing,[36] as energy storage materials

[a]i-Lab and Division of Nanobiomedicine, Suzhou Institute of Nano-tech and Nano-Bionics, Chinese Academy of Sciences, Suzhou, China 215123. E-mail: jjiang2010@sinano.ac.cn; Fax: +86-512-6260-3079; Tel: +86-512-6287-2662

[b]Institute of Biophysics, Chinese Academy of Sciences, Beijing, China 100101

[c]Graduate University of Chinese Academy of Sciences, Beijing, 100049, China

[d]State Key Laboratory of Multiphase Complex Systems, Institute of Process Engineering, Chinese Academy of Sciences, Beijing, China 100190. E-mail: jyang@mail.ipe.ac.cn; Fax: +86-10-8254 4814; Tel: +86-10-8254 4915

† Electronic supplementary information (ESI) available: TEM images, elemental line scan profiles of CuPt and Pt–CuS, and XRD of CuPt alloy NPs, and CO stripping results from Pt and Pt–CuS. See DOI: 10.1039/c3ta12049j

in lithium ion batteries and supercapacitors,[37,38] and as low cost photothermal therapeutic agents.[39,40] However, unlike other metal chalcogenides such as PbS (or PbSe) and CdS (or CdSe), reports on hybrids of Cu_xS and metals have been very limited. Park *et al.* have reported the synthesis of Au–Cu_2S core–shell nanoparticles and their enhanced photodegradation efficiency toward organic dyes under visible light irradiation compared to pure Cu_2S,[7] which was ascribed to the interfacial electron transfer from Cu_2S to Au domain, while hybrids between Cu_xS and other noble metals and their properties are yet to be explored.

Herein, we report the synthesis of heterostructured Pt–CuS from CuPt alloy nanoparticles using elemental sulfur, following the method and mechanistic insight developed from our previous report on synthesizing Au–Cu_2S heteromers by oxidation and *in situ* conversion of AuCu alloy nanoparticles using dodecanethiol.[30] The sizes of each domain in the hybrid can be independently controlled, and careful characterization of the obtained heterodimer structures revealed the existence of CuS with strong near IR absorption. Different from the reported results on pure PtCu alloy nanoparticles where both the methanol oxidation reactions[41] and oxygen reduction reactions[42] were enhanced compared to Pt alone, the electronic coupling between the two connecting domains strongly affected the catalytic properties of Pt, as the Pt–CuS heterodimer exhibited enhanced methanol oxidation properties compared to commercial Pt/C catalysts, while showing only low activity toward oxygen reduction reactions in stark contrast to Pt/C.

Experimental section

Materials

Octadecene (ODE, 90%) and copper(II) acetylacetonate (Cu(acac)$_2$, 99.99%) were purchased from Sigma-Aldrich. Platinum(II) acetylacetonate (Pt(acac)$_2$, Pt $\geq$ 48%) was purchased from Alfa Aesar. All other chemicals were purchased from Aladdin reagent company. All chemicals were used as received without further purification.

Synthesis of CuPt alloy nanocrystals

CuPt alloy nanocrystals were synthesized by a seeded-growth method under inert atmospheres using a standard Schlenk line, where Cu- and Pt-based routes were adopted with the following conditions, respectively.

Cu-based route. 10 nm Cu seeds were first prepared by reducing copper salt with oleylamine (OAm) following a published method,[43] which were then used for CuPt alloy nanoparticle formation. Typically, 50 mg Cu(acac)$_2$ was dissolved in 5 mL OAm with vigorous stirring. The solution was then heated up to 215 °C under the protection of nitrogen. After aging for two hours, 0.21 mmol H_2PtCl_6 was swiftly added into the dark red Cu nanoparticle solution, and the reaction mixture was held at 215 °C for two hours or further heated up to 250 °C for two hours. After that, the solution was cooled down to room temperature naturally and the CuPt alloy nanoparticles (NPs) were obtained by adding ethanol to the reaction mixture and centrifugation, which were further purified by washing with hexane/ethanol and centrifuging 2–3 times.

Pt-based route. Pt nanoparticles were first prepared following our previous report[44] as seeds for CuPt alloy formation. For Pt NP synthesis, 80 mg Pt(acac)$_2$ and 6 mg $AgNO_3$ were dissolved in 26 mL OAm. This mixture was heated up to 160 °C under nitrogen flow for three hours with vigorous stirring. Dark brown Pt NPs were obtained after washing and centrifuging with hexane and ethanol 2–3 times. The as acquired Pt NPs were then mixed with 50 mg Cu(acac)$_2$ in 16 mL OAm. After nitrogen flow for 30 min at room temperature, the mixture was heated to 120 °C at a rate of 10 °C min^{-1} and the reactants were held at this temperature for 30 min to remove water. Then the temperature was further raised to 230 °C at a ramp rate of 2 °C min^{-1} and aged for 90 min, after which the solution was cooled down to room temperature. The obtained CuPt NPs were again purified by washing with hexane and precipitating by adding ethanol.

Synthesis of Pt–CuS heterodimers from CuPt alloy NPs

The as acquired CuPt (0.05 mmol) alloy NPs were first dispersed and stirred in 3 mL ODE under nitrogen protection for 30 min. The mixture was then heated up to 130 °C at a ramp rate of 5 °C min^{-1}. After reaching the set temperature, 8 mg elemental sulfur dissolved in 1 mL 1,2-dichlorobenzene was swiftly injected into the solution and the solution was left to react for 10 min before cooling down to room temperature. The obtained NPs were washed with hexane and ethanol the same way as described in the above procedures.

Nanoparticle characterization

Transmission electron microscopy (TEM) images were taken using a FEI Technai G2 S-Twin at an accelerating voltage of 200 kV. TEM samples were prepared by drop-casting 1 to 2 drops of the nanoparticle hexane solution onto a carbon-coated Cu or Ni grid. UV-vis-NIR absorption spectra were recorded on a Lambda-25 spectrometer (PerkinElmer Inc., USA).

X-ray diffraction (XRD) analyses were performed using a Bruker D8 Advance X-ray diffractometer (with Cu Kα radiation at 0.15418 nm). X-ray photoelectron spectra (XPS) analyses were conducted on a PHI 5000 VersaProbe spectrometer (ULVAC-PHI) using Al Kα radiation (1486.71 eV).

Electrochemical measurements

Electrochemical measurements were carried out in a standard three-electrode cell connected to a Bio-Logic SAS VMP3 potentiostat/galvanostat. A leak-free Ag/AgCl (saturated with KCl) electrode was used as the reference electrode. The counter electrode was a platinum mesh (1 $\times$ 1 cm^2) attached to a platinum wire.

For the loading of the catalyst on a Vulcan XC-72 carbon support, a calculated amount of carbon powder was added to the hexane solution of Pt–CuS heterodimers obtained by the Pt-based route. After stirring the mixture for 24 h, the Pt–CuS/C (20 wt% Pt on carbon support) was collected by centrifugation,

washed thrice with methanol, and then dried at room temperature under vacuum.

The working electrode was a thin layer of Nafion-impregnated catalysts cast on a vitreous carbon disk. This electrode was prepared by ultrasonically dispersing 10 mg of the Pt–CuS/C in 10 mL of aqueous solution containing 4 mL of ethanol and 0.1 mL of Nafion solution. A calculated volume of the ink was dispensed onto the 5 mm glassy carbon disk electrode to produce a nominal catalyst loading of 20 μg cm^{-2} (Pt basis). The carbon electrode was then dried in a stream of warm air at 70 °C for 1 h.

The catalyst performance in room temperature methanol oxidation reaction (MOR) was evaluated by cyclic voltammetry. For these measurements, before the voltammograms were recorded, the potential window of 0 V to 1 V was scanned at 20 mV s^{-1} until a stable response was obtained. The electrolyte used was methanol (1 M) in perchloric acid (0.1 M). The current densities were normalized in reference to the geometric area of the glassy carbon electrode.

The catalyst performance in room temperature oxygen reduction reaction (ORR) was evaluated in $HClO_4$ electrolyte solution (0.1 M) using a glass carbon rotating disk electrode (RDE) at a rotation speed of 1600 rpm. Negative-going linear sweep voltammograms were recorded from 1 V to 0 V at 20 mV s^{-1} at room temperature in the presence of ultra-pure bubbling oxygen to maintain a saturated oxygen atmosphere near the working electrode. The current density was also normalized with the geometric area of the glassy carbon electrode.

Results and discussion

Synthesis of CuPt alloys

CuPt alloy NPs can be prepared by either a Cu-seeded or a Pt-seeded approach, where Cu or Pt nanoparticles were first prepared following literature reports, and the second metal was then reduced in the presence of the seed NPs, forming alloy NPs as shown in Scheme 1. Depending on the synthetic routes, CuPt alloy NPs with different sizes can be synthesized. Fig. S1† in the ESI displays the TEM images of CuPt alloy NPs obtained under different experimental conditions. The elemental line scan profile corresponding to CuPt alloy nanoparticles shows a rather homogeneous distribution of Cu and Pt (Fig. S2†), and the XRD pattern matched well with CuPt (JCPDS 42-1326), indicating successful synthesis of alloy NPs (Fig. S3 and S4†). It is clear from the TEM and XRD results that the size of CuPt alloy NPs is smaller when a Pt-seeded growth method was utilized, due to the relative large size of starting Cu seeds (~10 nm) compared to ~4 nm Pt seeds.

Synthesis and characterization of Pt–CuS heterodimers

Based on our previous study on synthesizing Au–Cu_2S hybrid NPs,[30] the heterostructured Pt–CuS NPs were obtained similarly by sulfidation of CuPt alloy NPs and subsequent phase segregation (Scheme 1). As the sizes of the starting alloy NPs were changed (Fig. S1†), the hybrid NP morphologies and sizes can be varied accordingly. As shown in Fig. 1 and Fig. 2a, 10–12 nm, 12–12 nm and 5–15 nm Pt–CuS heterodimers were prepared and imaged under TEM, the darker contrast domains being Pt NPs and the lighter ones being CuS NPs. Sulfidation of Cu-based CuPt which was aged at 215 °C produced hybrid NPs with truncated cube-like Pt domains (Fig. 1a), while those aged at 250 °C resulted in hybrid NPs with spherical Pt domains (Fig. 1b), likely a result of diffusion, restructuring and Oswald ripening of the alloy nanoparticles at different reaction temperatures. When the smaller Pt-based CuPt alloy NPs were used, hybrid NPs with smaller and spherical Pt domains were formed (Fig. 2a), and the elemental line scan profile confirms the composition and distribution of Pt, Cu, and S (Fig. S5†). The CuS domains in all three examples showed a plate-like morphology which can be clearly seen in Fig. 1, where some of the CuS nanoplates stand on their thin side planes. As nanoparticle catalytic property depends strongly on the surface to volume ratio, we will focus on the smaller Pt based hybrids for their following property studies.

The crystal structure of the Pt–CuS hybrid NPs (5–15 nm, Fig. 2a) was examined by X-ray diffraction study (Fig. 2b). Two series of Bragg reflections were found, which were ascribed to cubic-phase Pt (JCPDS 04-0802) and hexagonal CuS (JCPDS 65-0603) respectively. The well defined peaks in the XRD pattern indicate the formation of pure phase Pt and CuS with high

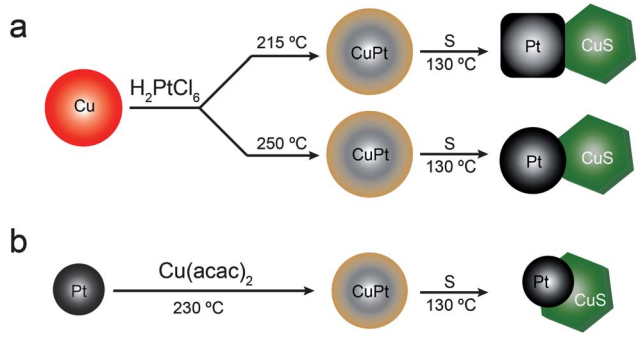

Scheme 1 Schematic drawing of CuPt alloy nanoparticle synthetic routes and experimental conditions (not drawn to scale): (a) Cu-based routes and (b) Pt-based synthesis, and their subsequent sulfidation process forming Pt–CuS heterodimers.

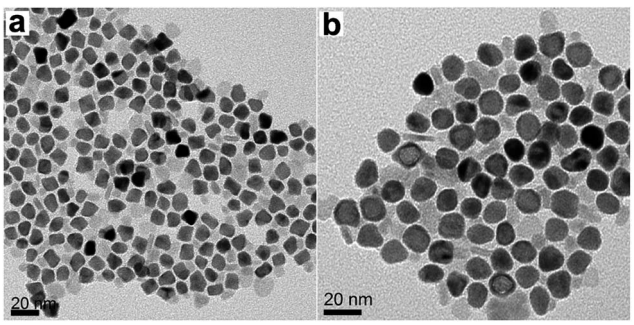

Fig. 1 TEM images of (a) 10–12 nm and (b) 12–12 nm Pt–CuS heterodimers prepared by changing CuPt alloy formation conditions as illustrated in Scheme 1a. (a) With Cu seeded CuPt alloy aged at 215 °C; (b) with Cu seeded CuPt alloy aged at 250 °C. Dark contrast domains are Pt NPs and the lighter ones are CuS NPs.

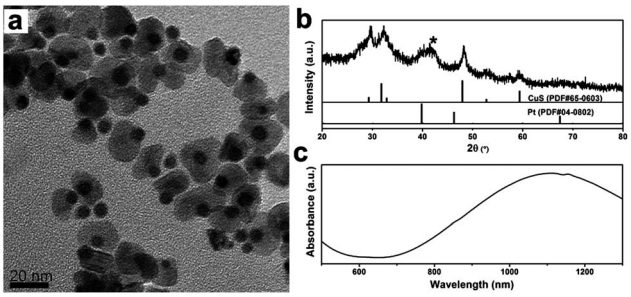

Fig. 2 Characterization of 5–15 nm Pt–CuS hybrids from Pt seeded alloy NPs. (a) TEM image; (b) X-ray diffraction pattern of Pt–CuS heterodimers, where the diffraction peaks can be indexed to cubic Pt and hexagonal CuS nanocrystals respectively, and the * indicates the diffraction peak from residual CuPt; (c) UV-vis-NIR absorption spectrum of Pt–CuS, the broad absorption peak in the near infrared window was due to the plasmonic absorption of non-stoichiometry CuS.

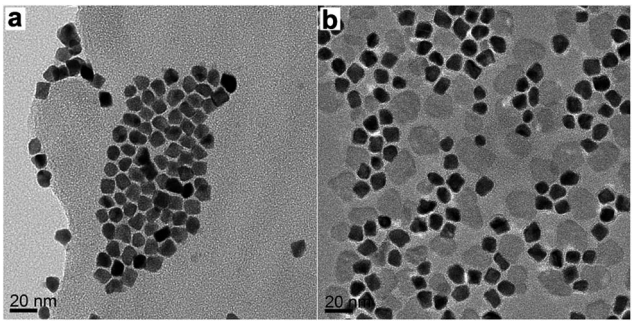

Fig. 3 Effect of reaction temperature on Pt–CuS hybrid NP formation. (a) Elemental sulfur was injected into CuPt alloy NPs at 90 °C, low yield Pt–CuS with small CuS domains were obtained; (b) elemental sulfur injection conducted at 190 °C, Pt–CuS hybrid NPs with large and irregular CuS domains ranging from 15 to 25 nm were observed.

crystallinity. However, a diffraction peak corresponding to residual CuPt was also observed (marked by * in Fig. 2b), which is due to incomplete de-alloying and subsequent sulfidation, and similar results were obtained with Se reacting with AuCd alloy nanoparticles.[45] The corresponding UV-vis spectrum was also recorded (Fig. 2c). The hybrid NPs exhibited a strong NIR absorption peak centered at ~1110 nm, which can be attributed to the plasmonic absorption of the non-stoichiometry CuS domain. As hole-doped semiconductor quantum dots, CuS was shown to exhibit localized surface plasmon resonances (LSPRs) in the NIR region.[32] These data all indicate the successful synthesis of Pt–CuS heterodimer NPs.

To better understand the formation process of Pt–CuS heterodimer NPs, the sulfidation process was monitored by observing reaction solution color changes. The reaction was rapid just as the formation of Au–Cu_2S hybrid NPs.[30] Immediately after the injection of sulfur, the solution color changed from dark brown to grey green, indicating that the sulfidation reaction occurred. As shown by the TEM image (Fig. 2a), elemental line scan profile (Fig. S5†) and XRD pattern (Fig. 2b), heterodimer NPs were formed with distinct Pt and CuS diffraction peaks, showing that the CuPt sulfidation process was completed within 10 min. The formation of heterodimers instead of core–shell nanoparticles was likely due to lattice mismatch between cubic phase Pt (3.92 Å) and hexagonal phase CuS (3.79 Å), as the formation of heterodimers reduces the interfacial area of two materials in the hybrid, circumventing the large interfacial strain of otherwise concentrically formed core–shell geometry. This result is consistent with findings from our earlier work[30] and others,[31] where Au–Cu_2S and Pt–Ag_2S all exhibited heterodimer structures.

Effect of temperature on the heterodimer formation

Among different reaction conditions, in addition to the effect of the starting CuPt alloy NPs, the reaction temperature plays another important role in influencing the morphologies and sizes of the hybrid NPs. Using CuPt alloy NPs from Cu seeds aged at 215 °C as an example, if the injection temperature of elemental sulfur solution was lowered to 90 °C from 130 °C, hybrid NPs with small CuS domain of low yield were obtained (Fig. 3a). When the injection of sulfur was conducted at a higher temperature (190 °C), polydisperse hybrid NPs were formed with less shape controllability, where Pt shaped from spherical to cube-like and with large CuS domains of irregular sizes ranging from 15 to 25 nm (Fig. 3b). From these results, it is clear that a suitable temperature is essential for morphology controlled Pt–CuS heterodimer NP synthesis. The reaction temperature affects many factors such as alloy NP sulfidation, metal–metal sulfide NP phase segregation, and interparticle ripening. At the right reaction temperature, a balanced sulfidation reaction and subsequent phase separation process would result in the heterodimer hybrid NPs with good monodispersity.

Effect of sulfur source on the heterodimer formation

In our previous study on Au–Cu_2S hybrid NP synthesis,[30] it was shown that both 1-dodecanethiol (DDT) and elemental sulfur could oxidize AuCu alloy NPs, with sulfur performing at a lower reaction temperature. It is worth noting that in the current CuPt system, 1-dodecanethiol cannot trigger CuPt sulfidation reaction as sulfur did here, even when the CuPt alloy NPs were exposed to an oxygenated atmosphere and the oxidizing temperature was raised to 200 °C. Under such extreme conditions, only irregular CuPt NPs with no heterodimers were observed under TEM (data not shown). This may be partly due to the higher stability of CuPt alloy NPs compared to AuCu alloy NPs, which made CuPt alloy sulfidation infeasible for DDT under similar experimental conditions.

All the above results on Pt–CuS heterodimer synthesis indicate that temperature and the reactivity of the sulfur source played key roles in inducing the sulfidation of Cu in CuPt alloy and subsequent phase segregation. Similar to our recent work on the Ag_2S-hollow Pt nanocomposites,[46] Cu was oxidized and reacted with S on the alloy nanoparticle surface, driving more Cu diffusing to the surface at elevated temperatures and forming CuS. Coupled with the restructuring and Oswald ripening of the de-alloyed Pt nanoparticles, Pt–CuS heterodimers with well defined structures were generated.

Selective catalytic activity toward methanol oxidation

The Pt–CuS hybrid heterodimers were examined for their electrocatalytic activities toward the room temperature methanol oxidation reaction (MOR) and benchmarked against the commercial Pt/C catalysts (E-TEK, 20 wt% 3.2 nm Pt nanoparticles on Vulcan XC-72 carbon support). Voltammograms of methanol oxidation were obtained in the potential window of 0−1 V at a sweep rate of 20 mV s^{-1} (Fig. 4a). The current densities in the voltammograms were normalized with the geometric area of the glassy carbon electrode. The peak current densities of Pt–CuS heterodimers associated with methanol oxidation in the forward and reverse scans were 10.87 mA cm^{-2} and 7.22 mA cm^{-2}, respectively, slightly higher than those of commercial Pt/C catalysts (10.43 mA cm^{-2} and 5.03 mA cm^{-2}, respectively). The comparison in current densities indicated that the Pt–CuS heterodimers showed greater activity for methanol oxidation than that of commercial Pt/C catalysts. In particular, the onset potential of methanol oxidation on Pt–CuS hybrid heterodimers was only ~0.2 V, much lower than that of commercial Pt/C catalysts (~0.3 V), indicating that the oxidation of methanol was much easier on Pt–CuS heterodimers than that on commercial Pt/C catalysts.

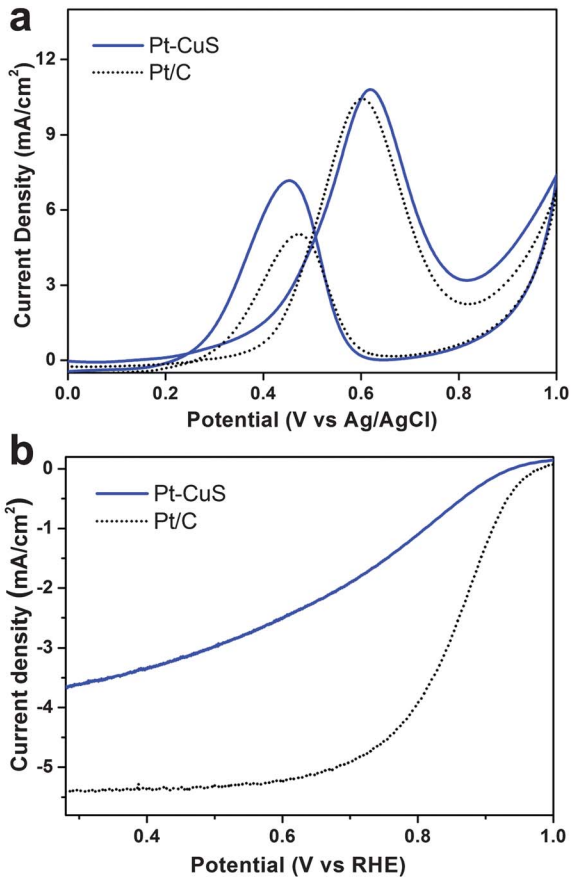

Fig. 4 (a) Cyclic voltammograms of Pt–CuS heterodimers (solid blue line) and commercial Pt/C catalysts (black dotted line) in argon-purged $HClO_4$ (0.1 M) with methanol (1 M) at room temperature. Sweep rate: 20 mV s^{-1}. (b) ORR polarization curves for the Pt–CuS heterodimers and commercial Pt/C catalysts (same plot legends as in a), recorded at room temperature in an O_2-saturated $HClO_4$ solution (0.1 M) at a sweep rate of 20 mV s^{-1} and a rotating speed of 1600 rpm.

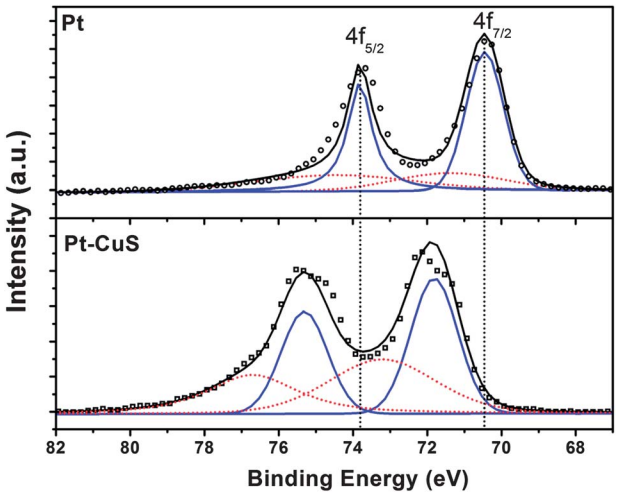

Fig. 5 Pt 4f XPS spectra of Pt (upper panel) and Pt–CuS heterodimer NPs (lower panel), where the binding energy increased 1.5 eV in the presence of CuS.

To understand the mechanism behind the enhancement of catalytic activity of Pt–CuS heterodimers for methanol oxidation, the X-ray photoelectron spectroscopy (XPS) Pt 4f spectra of Pt and Pt–CuS heterodimers were analyzed. Fig. 5 shows that the Pt 4f spectra can be deconvoluted into two pairs of doublets. The more intense doublet (at 70.4 and 73.8 eV for Pt, 71.8 and 75.3 eV for Pt–CuS) corresponded to Pt(0). The second and weaker doublet, with binding energies of ~1.4 eV higher than those of Pt(0), could be assigned to Pt(II) as in PtO and $Pt(OH)_2$.[47,48] Compared with the Pt $4f_{7/2}$ and $4f_{5/2}$ binding energies of pure Pt, an appreciable shift to higher values was observed in the Pt–CuS heterodimers, suggesting that electrons were transferred from Pt to CuS domains of the heterodimers. This electron-donating effect from Pt to CuS domains in Pt–CuS heterodimers could be explained by intra-particle charge transfer. A reversed charge transfer has been observed in the core–shell Au@PbS system, whereby the electrons transfer from the PbS shell to the inner Au core resulted in the n-type to p-type change in hydrazine-treated PbS.[49]

The catalytic feature of Pt–CuS heterodimers (blue solid line in Fig. 4a) indicated that the catalytic activity of Pt toward MOR can be enhanced by integrating with CuS, which could be interpreted by the electron coupling effect between Pt and CuS domains. As evinced by the XPS analyses (Fig. 5), the strong electron-withdrawing effect from CuS to the neighboring Pt domain induces an increase of 5d vacancies in Pt, resulting in an improvement of methanol adsorption on the surface of Pt sites, which is favourable for methanol oxidation. Analogous results were reported in bimetallic systems consisting Pt and transition metals, where Fe, Ni, or Co can enhance the O_2 adsorption on Pt by withdrawing electrons from neighbouring Pt atoms.[50] Similarly, in Co@Pt core–shell nanoparticles, compressive strain induced a downward shifting of the Pt d-band center, resulting in a balanced adsorption of CO and the dehydrogenation steps in the MOR process, thus enhancing the methanol oxidation process.[51] A low local density of electrons around Pt is generally associated with strong chemisorption, and this was further characterized by the

CO stripping test. Fig. S6† showed the CO stripping voltammograms of Pt–CuS heterodimers and commercial Pt/C catalysts after the working electrode has been held at −0.15 V for 30 min in CO saturated 0.1 M $HClO_4$. The CO stripping peaks of the Pt–CuS heterodimers shifted slightly to a more positive potential as compared to commercial Pt/C, indicating a little stronger adsorption of CO on Pt–CuS hybrid particles. This is consistent with the XPS analysis of the hybrid nanoparticles. The chemisorption of CO on Pt involves the donation of lone pair electrons from the filled carbon σ orbital of CO to the empty 5d orbital of Pt, which is compensated by the back donation of electrons from the Pt dπ orbital to the π^* orbitals of CO.[52] In future work, an oxophilic metal could be introduced to the Pt–CuS hybrid nanosystems to overcome the strong adsorption of CO while maintaining the improved adsorption of methanol for further enhancement of the MOR activity.

In contrast to their high catalytic activity for MOR, the Pt–CuS heterodimers exhibited poor activity for oxygen reduction reaction (ORR), another key reaction in DMFC.[53] Polarization curves for the ORR over commercial Pt/C catalysts and Pt–CuS heterodimers are presented in Fig. 4b. The half-wave potential for Pt–CuS heterodimers was 662 mV, only 77% of commercial Pt/C catalysts (855 mV). The kinetic current density at half-wave potential of heterodimers was also much lower than that of commercial Pt/C. The poor catalytic activity of the Pt–CuS heterodimers for ORR could also be attributed to the electron coupling effect between Pt and CuS domains in the heterodimers. It has been generally accepted that the common ORR process, *i.e.* the series 4 electron pathway, must involve both the breaking of an O–O bond and the formation of O–H bonds.[54–56] The most active Pt-based catalyst should have the optimal surfaces to facilitate both bond-breaking and bond-making steps without hindering one or the other.[57,58] However, in the Pt–CuS heterodimers, the surface of the Pt domain might be far from the optimal balance, and the Pt shells may suffer from hindered bond-breaking or bond-making steps, and therefore are less active than pure Pt/C catalysts. The strong electron-withdrawing effect from CuS to Pt induced an increase of 5d vacancies in Pt, increasing 2π electron donation from O_2 to the Pt surface. The O_2 adsorption on the Pt surface might be too strong for the formation of O–H bonds, which would account for the poor activity of Pt–CuS heterodimers toward ORR. It is noteworthy that the electronic coupling effect in the hybrid nanosystem is only the most possible explanation we proposed for the catalytic selectivity of Pt–CuS heterodimers toward MOR and ORR. The limitation of using this explanation is apparent, since the stability of elemental species involved, *e.g.* Cu and S, in the MOR/ORR reaction environment is not known and they might also play important roles in determining the catalytic activity of the heterodimers. Thorough particle characterization and elemental analysis are of necessity before the experimental data can be used to generalize even a phenomenological theory.

Conclusions

In summary, we have demonstrated a facile strategy for the synthesis of Pt–CuS nano-heterodimers, which involved the preparation of CuPt alloy nanoparticles in oleylamine, followed by the reaction with elemental sulfur in octadecene at elevated temperatures. The Pt–CuS heterodimers displayed highly selective activity for catalyzing the methanol oxidation reaction at room temperature due to the strong electronic coupling effect between the different domains in the heterodimers. By optimizing the domain sizes for the hybrid system through varying the ratio of metal precursors in alloy templates, further enhancement in MOR activity could be expected. This methodology should be valuable for the development of semiconductor–metal nanocomposites with interesting architectures and tailored functionalities that are difficult to synthesize by typical seed-mediated growth techniques.

Acknowledgements

This work is funded by the "Hundred Talents" program of Chinese Academy of Sciences, and CAS/SAFEA International Partnership Program for Creative Research Teams. We thank Dr Jinhua Yang at Institute of Bioengineering and Nanotechnology (Singapore) for helpful discussions.

Notes and references

1 X. Feng, Y. Chen and D. Hou, *Physica B*, 2011, **406**, 1702–1705.
2 Y. Li, Q. Zhang, A. V. Nurmikko and S. Sun, *Nano Lett.*, 2005, **5**, 1689–1692.
3 E. Shaviv and U. Banin, *ACS Nano*, 2010, **4**, 1529–1538.
4 J. Yang and J. Y. Ying, *Angew. Chem., Int. Ed.*, 2011, **50**, 4637–4643.
5 L. Amirav and A. P. Alivisatos, *J. Phys. Chem. Lett.*, 2010, **1**, 1051–1054.
6 R. Costi, A. E. Saunders, E. Elmalem, A. Salant and U. Banin, *Nano Lett.*, 2008, **8**, 637–641.
7 Y. Kim, K. Y. Park, D. M. Jang, Y. M. Song, H. S. Kim, Y. J. Cho, Y. Myung and J. Park, *J. Phys. Chem. C*, 2010, **114**, 22141–22146.
8 M. T. Sheldon, P. E. Trudeau, T. Mokari, L. W. Wang and A. P. Alivisatos, *Nano Lett.*, 2009, **9**, 3676–3682.
9 J. Yang, X. Chen, F. Ye, C. Wang, Y. Zheng and J. Yang, *J. Mater. Chem.*, 2011, **21**, 9088–9094.
10 D. Wang and Y. Li, *J. Am. Chem. Soc.*, 2010, **132**, 6280–6281.
11 G. Krylova, L. J. Giovanetti, F. G. Requejo, N. M. Dimitrijevic, A. Prakapenka and E. V. Shevchenko, *J. Am. Chem. Soc.*, 2012, **134**, 4384–4392.
12 C. Wang, W. Tian, Y. Ding, Y.-q. Ma, Z. L. Wang, N. M. Markovic, V. R. Stamenkovic, H. Daimon and S. Sun, *J. Am. Chem. Soc.*, 2010, **132**, 6524–6529.
13 G. Menagen, J. E. Macdonald, Y. Shemesh, I. Popov and U. Banin, *J. Am. Chem. Soc.*, 2009, **131**, 17406–17411.
14 J. Gao, B. Zhang, Y. Gao, Y. Pan, X. Zhang and B. Xu, *J. Am. Chem. Soc.*, 2007, **129**, 11928–11935.
15 Y. Feng, J. He, H. Wang, Y. Y. Tay, H. Sun, L. Zhu and H. Chen, *J. Am. Chem. Soc.*, 2012, **134**, 2004–2007.
16 H. Gu, R. Zheng, X. Zhang and B. Xu, *J. Am. Chem. Soc.*, 2004, **126**, 5664–5665.

17 J. Yang, J. J. Peng, Q. B. Zhang, F. Peng, H. J. Wang and H. Yu, *Angew. Chem., Int. Ed.*, 2009, **48**, 3991–3995.
18 J. Yang, H. I. Elim, Q. B. Zhang, J. Y. Lee and W. Ji, *J. Am. Chem. Soc.*, 2006, **128**, 11921–11926.
19 L. Carbone and P. D. Cozzoli, *Nano Today*, 2010, **5**, 449–493.
20 H. Wu, O. Chen, J. Zhuang, J. Lynch, D. LaMontagne, Y. Nagaoka and Y. C. Cao, *J. Am. Chem. Soc.*, 2011, **133**, 14327–14337.
21 K. S. Lee, R. M. Anisur, K. W. Kim, W. S. Kim, T.-J. Park, E. J. Kang and I. S. Lee, *Chem. Mater.*, 2012, **24**, 682–687.
22 A. Figuerola, A. Fiore, R. Di Corato, A. Falqui, C. Giannini, E. Micotti, A. Lascialfari, M. Corti, R. Cingolani, T. Pellegrino, P. D. Cozzoli and L. Manna, *J. Am. Chem. Soc.*, 2008, **130**, 1477–1487.
23 R. Buonsanti, V. Grillo, E. Carlino, C. Giannini, F. Gozzo, M. Garcia-Hernandez, M. A. Garcia, R. Cingolani and P. D. Cozzoli, *J. Am. Chem. Soc.*, 2010, **132**, 2437–2464.
24 K. Vinokurov, J. E. Macdonald and U. Banin, *Chem. Mater.*, 2012, **24**, 1822–1827.
25 T. Mokari, E. Rothenberg, I. Popov, R. Costi and U. Banin, *Science*, 2004, **304**, 1787–1790.
26 G. Dukovic, M. G. Merkle, J. H. Nelson, S. M. Hughes and A. P. Alivisatos, *Adv. Mater.*, 2008, **20**, 4306–4311.
27 Y. Vasquez, A. E. Henkes, J. Chris Bauer and R. E. Schaak, *J. Solid State Chem.*, 2008, **181**, 1509–1523.
28 Y. Yin, R. M. Rioux, C. K. Erdonmez, S. Hughes, G. A. Somorjai and A. P. Alivisatos, *Science*, 2004, **304**, 711–714.
29 N. E. Motl, J. F. Bondi and R. E. Schaak, *Chem. Mater.*, 2012, **24**, 1552–1554.
30 X. G. Ding, Y. Zou and J. Jiang, *J. Mater. Chem.*, 2012, **22**, 23169–23174.
31 D. Wang, X. Li, H. Li, L. Li, X. Hong, Q. Peng and Y. Li, *J. Mater. Chem. A*, 2013, **1**, 1587–1590.
32 Y. Zhao, H. Pan, Y. Lou, X. Qiu, J. Zhu and C. Burda, *J. Am. Chem. Soc.*, 2009, **131**, 4253–4261.
33 Y. Wu, C. Wadia, W. Ma, B. Sadtler and A. P. Alivisatos, *Nano Lett.*, 2008, **8**, 2551–2555.
34 Y. Zhao and C. Burda, *Energy Environ. Sci.*, 2012, **5**, 5564–5576.
35 Z. Cheng, S. Wang, Q. Wang and B. Geng, *CrystEngComm*, 2010, **12**, 144–149.
36 A. A. Sagade and R. Sharma, *Sens. Actuators, B*, 2008, **133**, 135–143.
37 J. S. Chung and H. J. Sohn, *J. Power Sources*, 2002, **108**, 226–231.
38 T. Zhu, B. Xia, L. Zhou and X. W. Lou, *J. Mater. Chem.*, 2012, **22**, 7851–7855.
39 T.-T. Zhuang, F.-J. Fan, M. Gong and S.-H. Yu, *Chem. Commun.*, 2012, **48**, 9762–9764.
40 Q. Tian, F. Jiang, R. Zou, Q. Liu, Z. Chen, M. Zhu, S. Yang, J. Wang, J. Wang and J. Hu, *ACS Nano*, 2011, **5**, 9761–9771.
41 B. Y. Xia, H. B. Wu, X. Wang and X. W. Lou, *J. Am. Chem. Soc.*, 2012, **134**, 13934–13937.
42 P. Strasser, S. Koh, T. Anniyev, J. Greeley, K. More, C. Yu, Z. Liu, S. Kaya, D. Nordlund, H. Ogasawara, M. F. Toney and A. Nilsson, *Nat. Chem.*, 2010, **2**, 454–460.
43 S. Uk Son, I. Kyu Park, J. Park and T. Hyeon, *Chem. Commun.*, 2004, 778–779.
44 J. Yang and J. Y. Ying, *J. Am. Chem. Soc.*, 2010, **132**, 2114–2115.
45 P. Guardia, K. Korobchevskaya, A. Casu, A. Genovese, L. Manna and A. Comin, *ACS Nano*, 2013, **7**, 1045–1053.
46 H. Liu, F. Ye, H. Cao, G. Ji, J. Y. Lee and J. Yang, *Nanoscale*, 2013, **5**, 6901–6907.
47 Z. Liu, J. Y. Lee, M. Han, W. X. Chen and L. M. Gan, *J. Mater. Chem.*, 2002, **12**, 2453–2458.
48 C. D. Wagner, A. V. Naumkin, A. Kraut-Vass, J. W. Allison, C. J. Powell and J. J. R. Rumble, in *NIST Standard Reference Database 20, Version 3.2 (Web Version)*.
49 J.-S. Lee, E. V. Shevchenko and D. V. Talapin, *J. Am. Chem. Soc.*, 2008, **130**, 9673–9675.
50 T. Toda, H. Igarashi, H. Uchida and M. Watanabe, *J. Electrochem. Soc.*, 1999, **146**, 3750–3756.
51 X. Zhang, H. Wang, J. Key, V. Linkov, S. Ji, X. Wang, Z. Lei and R. Wang, *J. Electrochem. Soc.*, 2012, **159**, B270–B276.
52 F. A. Cotton and G. Wilkinson, *Advanced Inorganic Chemistry*, Wiley-Interscience, New York, 1980.
53 A. S. Arico, S. Srinivasan and V. Antonucci, *Fuel Cells*, 2001, **1**, 133–161.
54 V. R. Stamenkovic, B. S. Mun, M. Arenz, K. J. J. Mayrhofer, C. A. Lucas, G. Wang, P. N. Ross and N. M. Marković, *Nat. Mater.*, 2007, **6**, 241–247.
55 V. R. Stamenkovic, B. Fowler, B. S. Mun, G. Wang, P. N. Ross, C. A. Lucas and N. M. Marković, *Science*, 2007, **315**, 493–497.
56 N. M. Marković and P. N. Ross, *Surf. Sci. Rep.*, 2002, **45**, 117–229.
57 J. Zhang, M. B. Vukmirovic, Y. Xu, M. Mavrikakis and R. R. Adzic, *Angew. Chem., Int. Ed.*, 2005, **44**, 2132–2135.
58 J. Zhang, M. B. Vukmirovic, K. Sasaki, A. U. Nilekar, M. Mavrikakis and R. R. Adzic, *J. Am. Chem. Soc.*, 2005, **127**, 12480–12481.

